Claudia Zimmermann (Autor)

Experimental investigation and computational modelling of thermal boundary layers in turbulent natural convection

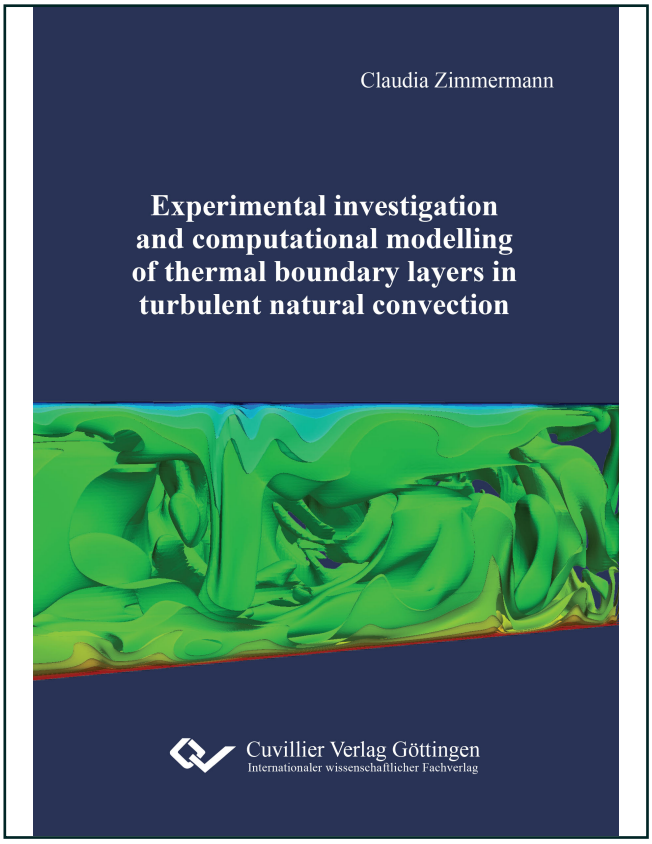

https://cuvillier.de/de/shop/publications/7034

1. Introduction

1.1. Motivation

Convective flows play an important role in many different areas, as, for example, in geology where these flows arise in the Earth's mantle causing a movement of the continental plates, the so-called *continental drift*. Convective flows are also used, to mention an example from another area, in form of passive cooling systems in industrial applications to reduce technical failures. Actually in everyday life, one can observe a convective flow, for example, during cooking a soup. Regarding a possible climate change, the understanding of these flows is especially important, because appearing as wind in the atmosphere they can result in a twister or even hurricane due to a Coriolis acceleration of the Earth's rotation.

If the convection is only driven by local density changes resulting from temperature differences inside the fluid, it is called a *natural convection*. In case of an additionally acting mechanical force, e. g. blower or pump, which drives the convection from outside, one would call it a *forced convection*.

1.2. Thesis purpose and outline

The main aspect of this thesis is the numerical investigation of a turbulent natural convection in *air* which is generated in different test case configurations between two opposite, isothermally heated walls. The focus of the investigation lies, beside the numerical modelling, on the understanding of the flow dynamic, the turbulence production and the fundamental fluid properties. Therefore, a compressible, 3-dimensional, transient, turbulent Large-Eddy Simulation (short: *LES*) without a Boussinesq-approximation is performed with help of the open-source software package *OpenFOAM®*. "Compressible" means in this case that density changes which are caused in the fluid by temperature differences are considered by the numerical model. "Compressible" does not include a definition in terms of the Mach number.

A compressible turbulence model is chosen, because, so far, incompressible models are not able to reflect fully the influence of varying density gradients on the turbulence production. Further, a compressible model is especially in one test case relevant due to an

intensified gravitational force field in this case. As turbulence model, the compressible model of *Fureby* is chosen which is a modification of the so called *Smagorinsky model* for compressible flows. Temperature dependent fluid properties are considered in all simulations by the *Sutherland model*.

The turbulent natural convective flows are analysed in three different test case configurations. Two of these test cases are numerically analysed (*VerCon* and *RayCon*) while the third one (*CenCon*) is investigated in an experimental study. The flow is limited in all setups by an enclosed rectangular container whose aspect ratios vary in each test case configuration. The container properties are chosen simplified to reduce especially complexity aspects. Nevertheless, they are still sufficient and commonly used regarding the investigation of fluid properties and flow structures in a turbulent natural convection.

The choice of the heated walls varies in all setups. The orientation of these walls relative to the effective direction of gravity effects significantly the profile of the main flow field inside the test case. The first setup (marked by *VerCon*) is made of a rectangular container where two of the vertical walls are heated isothermally, while both other cases (*RayCon* and *CenCon*) consist of a rectangular container where both horizontal walls are heated isothermally. Lateral walls of each setup are designed with different boundary conditions to analyse possible influences on the flow field inside the container.

The configurations of *RayCon* and *CenCon* are also called a *Rayleigh-Bénard problem* (short: RB problem). In contrast to *RayCon*, the setup of *CenCon* is additionally influenced by a Coriolis acceleration. The effect of the Coriolis acceleration is realised by a rotational movement of the test case under hyper-gravity in a large-scale centrifuge. While *CenCon* is rotating uniformly, possible influences on the flow structures, turbulence production and fluid properties due to the Coriolis acceleration should be investigated. All test cases are based on each other. The gained information and results of both first test cases, *VerCon* and *RayCon*, lead to the analyse of the third test case, *CenCon*.

The first main aspect in this thesis is the numerical investigation and understanding of the test cases *VerCon* and *RayCon*. Therefore, several fluid properties are estimated between the heated walls in each test case. Especially in the thermal boundary layer near these heated walls, the temperature as well as the velocity and Nusselt number profiles are important in order to understand the structure and dynamic of the flow and its turbulence production. The second main aspect is the numerical as well as experimental analysis of the influence of the Coriolis acceleration on the RB problem in the setup of *CenCon*.

Due to the vertical orientation of the heated walls in *VerCon*, the flow reaches a quasi-steady state after a while. This configuration of a turbulent natural convection represents the basis for both other test cases. Hence, it is very important and essential to study and understand first the flow dynamic and the behaviour of the fluid properties in this con-

figuration. The gained information and the at this point also validated numerical model of the chosen LES is required to analyse and understand both other cases.

The setup of *RayCon* is based directly on *VerCon* with its by 90° rotated heated walls. The setup of *CenCon* results from *RayCon* in its layout and in the realised flow dynamic as well as in the behaviour of the fluid properties regarding the state without a rotational movement of the test case. But, in contrast to *RayCon*, a rotation is additionally impressed on the setup which generates the additionally acting Coriolis acceleration. This realised relative acceleration affects the generated vertical convective flow inside the RB cell of *CenCon*. The conditions in the rotating setup of *CenCon* should simulate the atmospheric conditions in the beginning of a twister or hurricane. To generate these effects in the experimental setup without the help of additional air blowers, as they are used in other experimental setups, the radius of the centrifuge has to be sufficiently large, which is fulfilled in our case. The effect of the Coriolis acceleration is realised in the simulation by an implemented modified governing equation system (compared to the one of *RayCon*) which considers the additionally acceleration. *CenCon* is analysed at the end of this thesis on the basis of the beforehand obtained results of *RayCon*.

The numerical results of this thesis are validated to data of comparable experimental test cases as well as theoretical and numerical data from the literature. The realised Rayleigh-numbers lie in the range of $2.33 \times 10^6 \leq \mathrm{Ra} \leq 1.58 \times 10^9$. For *VerCon* it lies at $\mathrm{Ra} = 1.58 \times 10^9$, for *RayCon* between $6.16 \times 10^7 \leq \mathrm{Ra} \leq 4.1 \times 10^8$ and for *CenCon* between $2.33 \times 10^6 \leq \mathrm{Ra} \leq 4.32 \times 10^7$. The Prandtl number stays in each case at $\mathrm{Pr} = 0.71$ which represents the used fluid, air, in the chosen temperature intervals.

In the beginning of this thesis, the Navier-Stokes equations of a general compressible unsteady flow problem are presented. Outgoing from these equations, the governing equation system is derived which describes the observed turbulent natural convection. Subsequently, the computational methods and the mathematical model of the LES, which are used to solve the afore stated equations, are discussed. Before the particular test case configurations are explained in detail and the obtained results are demonstrated as main aspect of this thesis, the required thermodynamic properties of a turbulent natural convection are presented.

1.3. Related and previous studies

In the beginning of the 20th century, the French physicist *Henri Claude Bénard* (1874 - 1939) and the English physicist *Lord Rayleigh* (1842 - 1919) (former *John William Strutt*), performed the first analyses of a natural convection between two, horizontal, heated walls (see [Bénard1900], [Rayleigh1916]). This configuration of a natural convection is also called *Rayleigh-Bénard problem* named after both scientists. Since then, numerous studies in-

vestigating convective flow in different configurations were performed in an experimental, as well as a theoretical and a numerical way.

[Dafa'Alla1996] and [Betts00], for example, perform an experimental investigation of a low-level turbulent natural convection in air in a rectangular container with vertical heated walls and an aspect ratio of $\Gamma = 28.6$. While in the study of [Dafa'Alla1996] a Rayleigh number of $\mathrm{Ra} = 0.86 \times 10^6$ is realised, the study of [Betts00] investigates a Rayleigh number of $\mathrm{Ra} = 1.43 \times 10^6$ and one of $\mathrm{Ra} = 0.86 \times 10^6$. The main aspects of both studies lie on the temperature as well as velocity profiles between the heated walls. Based on the experimental study of [Dafa'Alla1996], [Versteegh1998] implements a *Direct Numerical Simulation* (short: DNS) for the same setup and for Rayleigh numbers between $5.4 \times 10^5 \leq \mathrm{Ra} \leq 5 \times 10^6$ and obtains an adequate approximation of the experimental results.

Furthermore, [Ziai1983], [Mergui1993], [Lankhorst1991] and [Tian00a], [Tian00b] analyse each a natural convection of a low-level turbulence in an experimental setup for different Rayleigh numbers. In [Tian00a], [Tian00b] a Rayleigh number of $\mathrm{Ra} = 1.58 \times 10^9$ is realised and in [Mergui1993] one of $\mathrm{Ra} = 1.7 \times 10^9$, while [Ziai1983] and [Lankhorst1991] investigate smaller values of $\mathrm{Ra} = 5 \times 10^8$ and $\mathrm{Ra} = 3.9 \times 10^8$. All studies examine mainly the profiles of the fluid properties between the heated walls in the vertical midplane, e. g. temperature and Nusselt number profiles. The experimental data in [Tian00a], [Tian00b] is used in the following to validate the numerical data of test case *VerCon* in chapter 5.

The opposite configuration of a natural convection between horizontal, heated walls, a Rayleigh-Bénard problem, was also the subject of many numerical as well as experimental studies in the last decade of years. One of the experimental studies can be found in [Funfschilling04] which investigates experimentally the plume motion and large-scale circulation in a methanol-filled cylindrical RB convection for Rayleigh numbers between $7 \times 10^7 \leq \mathrm{Ra} \leq 3 \times 10^9$ and a Prandtl number of $\mathrm{Pr} = 6$. One of the main goals of his study is the understanding of the periodically plume emission in the system. In [Maystrenko07] the boundary layer thickness in a RB convection in air in dependence on the fluid properties skewness and kurtosis is analysed. The convection cell has an aspect ratio of $\Gamma_x = 5$, $\Gamma_y = 1$ and the investigated Rayleigh numbers are $6 \times 10^7 \leq \mathrm{Ra} \leq 6 \times 10^8$.

Complementary to the previously mentioned study of [Maystrenko07], [Ebert08] measures in the same setup the temperature distribution and local heat flux density in air for Rayleigh numbers between $6.16 \times 10^7 \leq \mathrm{Ra} \leq 6.02 \times 10^8$ to obtain information about the local and global heat flux distribution mainly in the regions near the heated walls. In [Weiss11], a RB problem in a water-filled cylindrical cell with an aspect ratio of $\Gamma = 1/2$ is analysed for Rayleigh numbers between $2 \times 10^8 \leq \mathrm{Ra} \leq 1 \times 10^{11}$ as to the measurement of the Nusselt number and large scale circulation structures.

An example for a numerical study of a RB problem can be found in [Seiter1995], who models with help of a LES as well as a DNS a convective flow in air and in sodium generated between infinite horizontal channels. The Rayleigh numbers in this study lie at $\mathrm{Ra} = 2.5 \times 10^6$ and $\mathrm{Ra} = 10^7$. [Seiter1995] discusses the analysis of flow structures in the channels as well as the statistical evaluation of fluid properties for small Prandtl numbers. [Reeuwijk08a] and [Reeuwijk08b] investigate, with help of a DNS and periodic boundary conditions, the kinematic boundary layer and the heat flux in a RB configuration for an aspect ratio of $\Gamma = 4$, different Rayleigh numbers between $10^5 \leq \mathrm{Ra} \leq 10^8$ and a Prandtl number of $\mathrm{Pr} = 1$.

Shiskina et al. concentrate in [Shishkina06, Shishkina08, Shishkina09] mainly on three-dimensional, time-dependent DNS and well-resolved LES of turbulent RB problems in air and water using a Boussinesq-approximation. The test case consists of a wide cylindrical container. The realised Rayleigh numbers lie between $10^5 \leq \mathrm{Ra} \leq 10^{10}$. The main goals of these studies are the investigation of the thermal dissipation rate and the interaction of thermal plumes.

Similar to the previous studies, the study in [Silano10] performs in his study a DNS, using a Boussinesq-approximation, of a cylindrical cell with an aspect ratio of $\Gamma = 1/2$ for a range of Prandtl numbers between $10^{-1} \leq \mathrm{Pr} \leq 10^4$ as well as Rayleigh numbers between $10^5 \leq \mathrm{Ra} \leq 10^9$. The main goal of this study lies in the understanding of Nusselt-Reynolds-number dependencies in relation to the chosen Rayleigh and Prandtl numbers. Furthermore, *van der Poel et al.* investigate in [Poel13] differences between a 2- and a 3-dimensional RB convection in a cylindrical cell with varying aspect ratios for Prandtl numbers of $\mathrm{Pr} = 4.38$ and $\mathrm{Pr} = 0.7$ up to a Rayleigh number of $\mathrm{Ra} = 10^8$. Therefore, numerical results are compared to experimental data. The main aspect in this study are the Nu(Ra)- and also the Nu(Pr)-dependencies. Similarities between the 2D- and 3D-convection can be found for some parameter ranges. But also large differences are revealed, mainly for the case of $\mathrm{Pr} < 1$ and low aspect ratios, which have a significant effect on the Nusselt and Reynolds number distribution in the 2D-convection.

Complementary to the previously mentioned studies, [Ahlers06] searches experimentally and theoretically for differences between a convection with and without a Boussinesq-approximation. A natural convection for which a Boussinesq-approximation is assumed is called Oberbeck-Boussinesq (short: OB) convection, while a natural convection without a Boussinesq-approximation is called non-Oberbeck-Boussinesq (short: NOB) convection. The realised Rayleigh numbers lie in [Ahlers06] between $10^8 \leq \mathrm{Ra} \leq 10^{11}$. The cylindrical cell has an aspect ratio of $\Gamma \approx 1$. The study investigates the convection in water and in glycerol.

Considering an analytical formulation describing a natural convection, the possibly first approach to a formulated law of the turbulent boundary layer in the near wall region in a

natural convection can be found in [George1979]. For the laminar region of the boundary layer an analytical function can be found in [Pohlhausen1921]. *Pohlhausen* states in his study a solution for a flow over an infinitely long plate.

In the last years, the studies of [Hölling05, Hölling06] discuss analytical functions describing the turbulent thermal and velocity boundary layer in a natural convective flow for different ranges of Rayleigh as well as Prandtl numbers. The theory is valid for a configuration with vertical or for one with horizontal, heated walls. [Grossmann00, Grossmann01] describe in their studies possible Rayleigh-Nusselt-number-dependencies of strong RB problems valid in different regimes in the Rayleigh number versus Prandtl number phase space. The resulting power laws and defined regimes are discussed and updated in the study of [Stevens13].

Regarding studies which deal also, as it is the case in this thesis, with a Coriolis force influence, the studies of [Brown08a] and [Brown08b] can be mentioned. In both studies measurements of large-scale circulations are performed in several water-filled cylindrical convection cells of an aspect ratio of $\Gamma = 1$ and for $\mathrm{Pr} = 4.38$. In [Brown08a] the analysed Rayleigh numbers lie between $3 \times 10^8 \leq \mathrm{Ra} \leq 10^{11}$, while they lie at $\mathrm{Ra} \geq 10^{10}$ in the second study [Brown08b]. The experiments in [Brown08a] investigate the angular orientation of a turbulent large scale circulation as a function of time. In [Brown08b] the influence of a Coriolis force (caused by the Earth's rotation) on the development of large-scale structures is investigated over several days periods. The results show clockwise and counter-clockwise revolutions of the circulation plane orientation.

In the study of [Horn11], on the one hand, a three-dimensional DNS of a NOB convection is compared to one of an OB convection in a cylindrical cell of an aspect ratio of $\Gamma = 1$. The cell is filled with water ($\mathrm{Pr} = 4.38$) and the investigated Rayleigh number lies at $\mathrm{Ra} = 10^8$. The results show an asymmetrical temperature profile in the NOB convection as well as higher mean temperatures in the geometry centre than in case of the OB convection. On the other hand, an additional influence of a rotational movement of the NOB convection is analysed. The rotational movement of the cell leads to higher Nusselt numbers compared to a non-rotating cell.

To model mathematically a turbulent natural convection in a numerical simulation, different approaches can be found in the literature. The American meteorologist *Joseph Smagorinsky* was the first who formulated a turbulence model based on a formulation of the eddy viscosity, see [Smagorinsky1963]. The model uses also the assumption of a Boussinesq-approximation. The Smagorinsky model is widely used in LES methods and it is also the basis for several other turbulence models, as in [Germano1991, Lilly1992]. Both studies modify the Smagorinsky model to a dynamic version. In the study of [Fureby1996] a modified version of the Smagorinsky model is formulated for compressible flows. The study of [Deardorff1973] discusses the choice of the grid filter length in connection with

the Smagorinsky model concerning the use of subgrid transport equations for atmospheric turbulence.

To obtain a successful performance of a LES, the turbulent Prandtl number has to be chosen carefully in the turbulence model. Therefore, several studies on this topic can be found. For example, a suggestion of a turbulent Prandtl number in combination with an unstructured grid can be found in [Okong'O 00] or also in [Kosović02, Sergent03, Erlebacher1992] who develop new subgrid scale models. In [Kosović02, Erlebacher1992] turbulence models are presented which can be applied on compressible flows without using a Boussinesq-approximation. Furthermore, [Kenjereš1999, Sergent03] demonstrate turbulence models which use additional force terms to describe a turbulent natural convection.

In comparison to the mentioned related studies, in this thesis a compressible well-resolved LES is performed to model numerically a turbulent natural convection in air in three different test case setups. In each test case a different Rayleigh number range is analysed. In one test case, the natural convection is generated between two vertical, heated walls. In both other test cases a RB convection is realised (two horizontal, heated walls). The chosen computational grid of each test case is high-resolved, especially in the near wall regions. But all used computational grids consists of a smaller number of cells than it would be the case in a DNS.

The used compressible turbulence model is based on the mentioned model of Fureby in [Fureby1996]. Compared to most of the above related studies, the mathematical model of this thesis deals with the assumption of a non-Boussinesq fluid to investigate possible differences to the studies which consider a Boussinesq-approximation. Outstanding is the third test case, in which the influence of a Coriolis force on the development of turbulent as well as large-scale structures inside the fluid is analysed numerically as well as in an experimental study. The influence of the Coriolis acceleration is realised in the experiment by a rotational movement of the test case in a large scale centrifuge.

Note that some of the presented contents of this thesis are also discussed in extracts in the articles [Zimmermann12], [Zimmermann14a], [Zimmermann14b] and [Zimmermann15].

1.4. Conservation of mass

To describe a flow problem by a mathematical model, the flow properties and its movement have to be formulated by appropriate equations. These equations have to determine the *kinematic* as well as *transport* and *thermodynamic* properties of the flow. The first mentioned group includes properties of the flow field, e. g. velocity and angular velocity, while the two other mentioned groups describe properties of the fluid itself, e. g. frictional tensions or thermal diffusion and pressure, density or temperature. Next to the

description of the continuity motion also the thermodynamic properties like diffusion, momentum and heat transfer have to be formulated. The equations of viscous flows are well known in fluid dynamics. At this point, they are presented in their basic form for a three-dimensional flow problem. The following demonstrations are based on [Spurk07], chapter 1 and 2 and [White1991], chapter 1 and 2. The governing equations which model the flow properties and its movement are derived in the following from an infinitesimal small and finitely large fluid control volume Ω, as is indicated in figure 1.1. The following evaluations are done based on the information in [Spurk07], chapter 1, 1.2.1-1.2.5.

The control volume is separated from the rest of the fluid by a closed surface $\partial\Omega$. The volume consists of a set of infinitely many fluid particles, which are denoted by the set $\tilde{M}$. To model the movement of the flow, it has to be possible to identify the set of fluid particles in time and space. From the movement of the fluid particles in Ω, the movement of the whole flow can be concluded on the macroscopic level. The fluid volume is assumed to be *celestial*. Further, it is assumed as *continuum*. Hence, each fluid particle can be considered as material particle and the density as continuous function of time and position. Note, that the continuity assumption must not be fulfilled in every technical flow problem.

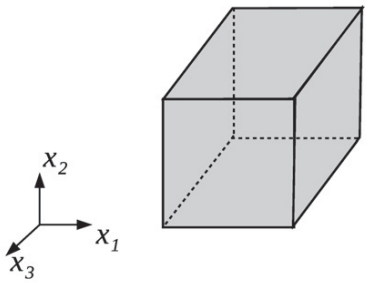

Figure 1.1.: Fluid control volume Ω (as seen in [Oertel06]).

The form of each fluid particle is variable in time and can change continually. Therefore, one particle has to be identified not by its form, but by a specified vector $\boldsymbol{\chi}$, which is characteristic for each particle. The movement of one particle can then be characterised at a time instant t_0 by its position vector $\boldsymbol{x}$ in relation to a chosen origin of a particular three-dimensional coordinate system

$$\boldsymbol{\chi} = \boldsymbol{x}(t_0)\,. \tag{1.4.1}$$

Or for the whole flow

$$\boldsymbol{x} = \boldsymbol{x}(\boldsymbol{\chi}, t)\,, \quad \text{or} \quad x_i = x_i(\chi_j, t) \quad \text{with} \quad i, j = 1, 2, 3\,. \tag{1.4.2}$$

Note, that $\boldsymbol{\chi}$ is a time independent vector. Equation (1.4.2) formulates a mapping between the referenced configuration at a time instant t_0 to the actual one at time t. The

formulation with $\boldsymbol{\chi}$ and time t is called *material description* or *Lagrangian description*, where $\boldsymbol{\chi}$ is the *material coordinate*. The velocity and acceleration of one fluid particle can be formulated in terms of $\boldsymbol{\chi}$ by

$$u_i(\chi_j, t) = \left[\frac{\partial x_i}{\partial t}\right]_{\chi_j}, \quad a_i(\chi_j, t) = \left[\frac{\partial u_i}{\partial t}\right]_{\chi_j}, \quad \text{with} \quad i, j = 1, 2, 3\,. \tag{1.4.3}$$

The index χ_j specifies the deviation for the χ_j-th point in the material. The first equation in (1.4.3) is called the *material* deviation of the velocity.

For the most problems in fluid mechanics, the above material notation is modified, to describe the flow at a specific location $\boldsymbol{x}$ and time t and not any longer in the material coordinate. With (1.4.3) each material coordinate can be transformed to the independent variables of a field coordinate $\boldsymbol{x}$ and time t. This transformation between both vectors is a *bijective* function (one-to-one correspondence). Equation (1.4.2) can then be rewritten as

$$\boldsymbol{\chi} = \boldsymbol{\chi}(\boldsymbol{x}, t)\,, \tag{1.4.4}$$

which describes the material point, which is at the place $\boldsymbol{x}$ at time t. The transformation for the velocity between both vectors is then

$$\boldsymbol{u}(\boldsymbol{\chi}, t) = \boldsymbol{u}\left[(\boldsymbol{\chi}(\boldsymbol{x}, t), t\right] = \boldsymbol{u}(\boldsymbol{x}, t)\,. \tag{1.4.5}$$

The notation in the field coordinate $\boldsymbol{x}$ and time t is called *field* or *Euler's description*. This notation describes the path of one particle at a time instant t and hence its position at t.

Sometimes it is more important to describe the changes of a material particle, and not the change in time at a given location. The change of $\boldsymbol{u}(\boldsymbol{x}, t)$ at $\boldsymbol{x}$ is not in every case the acceleration, which the material point felt in $\boldsymbol{x}$ at time t, e.g. for the case of a steady flow where the change of the velocity is zero at a specified location. If a material point proceed from $\boldsymbol{x}$ to $\boldsymbol{x} + d\boldsymbol{x}$, where $d\boldsymbol{x}$ is an element of the path line, it felt a change in $\boldsymbol{u}(\boldsymbol{x}, t)$, If the velocity is given in material coordinates, then the material derivative is given by (1.4.3), as mentioned before. If the velocity is described in field coordinates $\boldsymbol{u}(\boldsymbol{x}, t)$, the material derivative with respect to t can be formulated for a fixed $\boldsymbol{\chi}$ as

$$\frac{d\boldsymbol{u}}{dt} = \left[\frac{\partial \boldsymbol{u}\left(\boldsymbol{x}(\boldsymbol{\chi}, t), t\right)}{\partial t}\right]_{\boldsymbol{\chi}}. \tag{1.4.6}$$

In equation (1.4.6), the position $\boldsymbol{x}$ in $\boldsymbol{u}(\boldsymbol{x}, t)$ is replaced by the path coordinates of the fluid particle which is located in $\boldsymbol{x}$ at time t. The conservation of mass, momentum and energy have to be fulfilled in the following. The evaluation of the continuity equation is discussed in the following based on [Spurk07], chapter 1, 1.2.5 and chapter 2. The form

of the control volume varies during the motion. The region in space to which the volume is extended at time t, is denoted by $\Omega(t)$. The total mass m in the bounded volume Ω is determined by the sum of the particular material elements dm over the set of all material particles $\tilde{M}$

$$m = \int_{\tilde{M}} dm = \int_{\Omega(t)} \rho(\boldsymbol{x}, t)\, d\Omega \tag{1.4.7}$$

with the continuous function of space of density $\rho(\boldsymbol{x}, t)$. Note, that $\tilde{M}$ should consists the whole time of the same set of material points. Equation (1.4.7) can also be formulated for an arbitrary continuous function φ over a region $\Omega(t)$ in space

$$\int_{\tilde{M}} \varphi(\boldsymbol{\chi}, t)\, dm \; = \int_{\Omega(t)} \varphi(\boldsymbol{x}, t)\rho(\boldsymbol{x}, t)\, d\Omega. \tag{1.4.8}$$

In the following, the dependence on the coordinates is omitted and it infers from the range of each given integral. The mass in the bounded fluid volume has to be constant in time due to the conservation of mass. Hence, this is fulfilled for each mass particle in $\tilde{M}$

$$\frac{D}{Dt} m = 0\,, \qquad \frac{D}{Dt}(dm) = 0\,, \tag{1.4.9}$$

where $\dfrac{D}{Dt}$ denotes the *material derivative* in time. With the connection in (1.4.9), the fact, that φ is continuously differentiable and regarding the *Leibniz rule* (for further information see [Heuser09], chapter 4), the variation rate in time of equation (1.4.8) is subsequently

$$\frac{D}{Dt} \int_{\tilde{M}} \varphi\, dm \; = \frac{D}{Dt} \int_{\Omega(t)} \varphi\rho\, d\,\Omega \; = \int_{\Omega(t)} \frac{D}{Dt}(\varphi\rho)\, d\,\Omega. \tag{1.4.10}$$

Due to the Leibniz rule, the derivation of a continuously differentiable function can be done “under” the integral. An equivalent expression to (1.4.10) is

$$\frac{D}{Dt} \int_{\Omega(t)} \varphi\, d\,\Omega \; = \int_{\Omega} \frac{D}{Dt}\varphi\, d\,\Omega + \int_{\Omega} \varphi \frac{D}{Dt}(\, d\,\Omega). \tag{1.4.11}$$

Without loss of generality, the variable domain $\Omega(t)$ can be replaced by a fixed domain Ω which coincides with $\Omega(t)$ at time t, for the detailed derivation of (1.4.11) see [Spurk07], chapter 1, 1.2.5. Regarding equation (1.4.11), also the following formulation is valid

$$\frac{D}{Dt} \int_{\Omega(t)} \varphi\, d\Omega = \int_{\Omega} \left(\frac{\partial \varphi}{\partial t} + \frac{\partial \varphi u_i}{\partial x_i} \right) d\Omega\,, \tag{1.4.12}$$

where $\dfrac{\partial}{\partial t}$ denotes the partial derivative in time. Due to the fact, that φ is continuously differentiable in Ω, application of the theorem of Gauss (for further details to Gauss's theorem see [Amann08], chapter 3) on (1.4.12) produces the so-called *Reynolds' transport theorem*

$$\frac{D}{Dt}\int_{\Omega(t)} \varphi \, d\Omega = \int_{\Omega} \frac{\partial \varphi}{\partial t} \, d\Omega + \int_{\partial\Omega} \varphi \boldsymbol{u} \cdot \boldsymbol{n} \, dA \,, \tag{1.4.13}$$

where $\partial\Omega$ is the orientated bounded surface of Ω and $\boldsymbol{n}$ its normal vector. The Reynolds' transport theorem expresses the variation rate in time of the material volume integral to the rate of change of an arbitrary quantity φ, which is expressed in terms of the integral over Ω and in terms of its flux trough the bounded surface $\partial\Omega$ of Ω. At a time instant t, both control volumes Ω and $\Omega(t)$ coincide with each other (see [Spurk07], chapter 2, 2.1).

As mentioned above, the mass in the fluid volume should be time independent and constant. Regarding equation (1.4.12) with $\varphi = \rho$ the conservation of mass in (1.4.9) is transformed to

$$\frac{Dm}{Dt} = \frac{D}{Dt}\int_{\Omega(t)} \rho \, d\Omega = \int_{\Omega} \left(\frac{\partial \rho}{\partial t} + \frac{\partial \rho u_i}{\partial x_i} \right) d\Omega \, = 0 \,. \tag{1.4.14}$$

Because the range of the integral Ω is chosen arbitrarily, it can be concluded, that the continuous integrand must vanish and the conservation of mass can be formulated in its *differential* form

$$\frac{\partial \rho}{\partial t} + \frac{\partial \rho u_i}{\partial x_i} \tag{1.4.15}$$

or

$$\frac{\partial \rho}{\partial t} + \nabla \cdot (\rho \boldsymbol{u}) \,. \tag{1.4.16}$$

Equation (1.4.15) is also called *continuity equation*. If the fluid is a steady flow, it is $\dfrac{\partial \rho}{\partial t} = 0$ and equation (1.4.16) becomes

$$\nabla \cdot (\rho \boldsymbol{u}) \, = 0 \,. \tag{1.4.17}$$

If the volume is not variable in time $\dfrac{\partial \rho}{\partial t} = 0$ and space $\dfrac{\partial \rho}{\partial x} = 0$, the fluid is called *incompressible* and it is

$$\nabla \cdot \boldsymbol{u} \, = 0 \,. \tag{1.4.18}$$

1.5. Conservation of momentum

The next step in this section is the derivation of the momentum balance in the fluid volume Ω. Therefore, preliminary considerations are made. A fluid particle is able to perform four different types of motion or deformation as *translation*, *rotation*, *shear strain* and *extensional stresses*. The first two motions change only the location of the fluid particle, while both last motions modify also its form. The following demonstrations are based on [White1991], chapter 1, 1-3 (especially 1-3.3) and chapter 2, 2.4 as well as [Spurk07], chapter 2, 2.2. The motion is always associated to a change in time. The *translation* is

characterised by a displacement from one to another location $u_x\,dt$, $u_y\,dt$, $u_z\,dt$ of the particle (see as well figure 1.1). A *rotation* can be described by a motion of the fluid volume around a specified rotation axis in a particular angle α. Hence, the rate of the rotation is determined as

$$\frac{\partial\tilde{\Omega}_x}{dt} = \frac{1}{2}\left(\frac{\partial u_z}{\partial y} - \frac{\partial u_y}{\partial z}\right), \quad \frac{\partial\tilde{\Omega}_y}{dt} = \frac{1}{2}\left(\frac{\partial u_x}{\partial z} - \frac{\partial u_z}{\partial x}\right), \quad \frac{\partial\tilde{\Omega}_z}{dt} = \frac{1}{2}\left(\frac{\partial u_y}{\partial x} - \frac{\partial u_x}{\partial y}\right). \tag{1.5.1}$$

Expression (1.5.1) can be summarised as follows

$$\tilde{\boldsymbol{\omega}} = 2\frac{d\tilde{\boldsymbol{\Omega}}}{dt}. \tag{1.5.2}$$

$\tilde{\boldsymbol{\omega}}$ is called *vorticity* of the fluid and can be connected to the velocity by

$$\tilde{\boldsymbol{\omega}} = \nabla \times \boldsymbol{u}, \quad [\tilde{\boldsymbol{\omega}}] = \frac{1}{s}. \tag{1.5.3}$$

Then it is

$$\nabla \cdot \tilde{\boldsymbol{\omega}} = \nabla \cdot (\nabla \times \boldsymbol{u}) = 0. \tag{1.5.4}$$

If $\tilde{\boldsymbol{\omega}} = 0$, the flow is called *irrotational*.

The *shear strain* is characterised as the averaged angle between two lines of the fluid volume which were normal orientated to each other in the unstrained state. The shear strain rate is defined by

$$\epsilon_{xy} = \frac{1}{2}\left(\frac{\partial u_y}{\partial x} + \frac{\partial u_x}{\partial y}\right), \quad \epsilon_{yz} = \frac{1}{2}\left(\frac{\partial u_z}{\partial y} + \frac{\partial u_y}{\partial z}\right), \quad \epsilon_{zx} = \frac{1}{2}\left(\frac{\partial u_x}{\partial z} + \frac{\partial u_z}{\partial x}\right). \tag{1.5.5}$$

Consequently, the strain rates are symmetrical $\epsilon_{ij} = \epsilon_{ji}$. The *extensional strain* can be explained as an increase in the fluid particle's length

$$\epsilon_{xx} = \frac{\partial u_x}{\partial x}, \quad \epsilon_{yy} = \frac{\partial u_y}{\partial y}, \quad \epsilon_{zz} = \frac{\partial u_z}{\partial z} \tag{1.5.6}$$

or

$$\epsilon_{ij} = \begin{pmatrix} \epsilon_{xx} & \epsilon_{xy} & \epsilon_{xz} \\ \epsilon_{yx} & \epsilon_{yy} & \epsilon_{yz} \\ \epsilon_{zx} & \epsilon_{zy} & \epsilon_{zz} \end{pmatrix}. \tag{1.5.7}$$

ϵ_{ij} is a symmetric second-order tensor with the following invariants

$$\begin{aligned} I_1 &= \epsilon_{xx} + \epsilon_{yy} + \epsilon_{zz}, \\ I_2 &= \epsilon_{xx}\epsilon_{yy} + \epsilon_{yy}\epsilon_{zz} + \epsilon_{zz}\epsilon_{xx} - \epsilon_{xy}^2 - \epsilon_{yz}^2 - \epsilon_{zx}^2, \\ I_3 &= \begin{vmatrix} \epsilon_{xx} & \epsilon_{xy} & \epsilon_{xz} \\ \epsilon_{yx} & \epsilon_{yy} & \epsilon_{yz} \\ \epsilon_{zx} & \epsilon_{zy} & \epsilon_{zz} \end{vmatrix}. \end{aligned} \tag{1.5.8}$$

In Newton mechanics, a system is denoted as *inertial*, if its axes are fixed and Newtons first law of motion is satisfied. This implies, that the velocity of an object is constant in the system, if the object is not affected by any forces. Either the object is at a rest or it is moving linearly with a constant velocity (see [Nolting13], chapter 2, 2.2.3). In an inertial system, the variation rate in time of the momentum $\boldsymbol{I} = m\boldsymbol{u}$ equals the sum of all forces $\boldsymbol{F}_k$, which are acting on the system. Thus, for the fluid volume it has to be

$$\frac{D\boldsymbol{I}}{Dt} = \frac{Dm\boldsymbol{u}}{Dt} = \boldsymbol{F} = \sum_k \boldsymbol{F}_k\,, \quad \Rightarrow \quad m\boldsymbol{a} = \boldsymbol{F}\,, \tag{1.5.9}$$

which is *Newtons second law*. $\boldsymbol{a}$ is the acceleration of the fluid particle of mass m. Regarding the density instead of the mass, equation (1.5.9) is written as

$$\rho\frac{D\boldsymbol{u}}{Dt} = \boldsymbol{f} = \boldsymbol{f}_{\text{body}} + \boldsymbol{f}_{\text{surface}} \tag{1.5.10}$$

with the velocity $\boldsymbol{u}$ of the fluid particle and the applied force per unit volume $\boldsymbol{f}$, which acts on the fluid particle. The forces which impact on the fluid particle are divided in two classes, *body forces* and *surface forces*. A body force is usually applied to the entire mass and is impressed by an external field, e. g. the gravitational force $\boldsymbol{g}$. The surface forces are applied by external stresses which result from the surrounding fluid. The whole force, which is acting on the observed fluid volume can be described with help of equation (1.5.10) by an integration over the volume and its surface. The following demonstrations are based on [Spurk07], chapter 2, 2.2. It is

$$\mathbf{F} = \int_{\Omega(t)} \boldsymbol{k}\rho\, d\Omega + \int_{\partial\Omega(t)} \boldsymbol{t}\, d\partial\Omega\,. \tag{1.5.11}$$

The vector $\boldsymbol{k}$ stands for the body forces and the vector $\boldsymbol{t}$ is the so-called *deformation tensor* which compromises the surface forces. The deformation tensor is dependent on space, time and from the orientation of the normal vector $\boldsymbol{n}$ of the surface element. The deformation tensor is a linear combination of the components of $\boldsymbol{n}$. With the Einstein notation it is

$$t_j(\boldsymbol{x}, \boldsymbol{n}, t) = \tau_{ij}(\boldsymbol{x}, t)n_i \quad \text{with} \quad i, j = 1, 2, 3\,, \tag{1.5.12}$$

which is illustrated in figure 1.2. τ_{ji} stands for the magnitude of the i-th component of the deformation tensor, which effects the element of the coordinate plane with the normal vector, which points in the j-th direction.

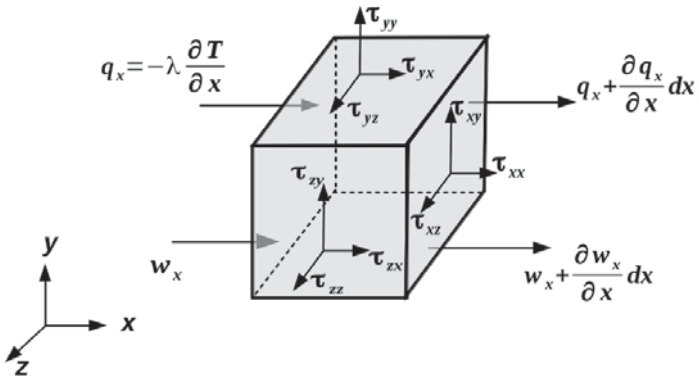

Figure 1.2.: Fluid volume with notation for stresses, heat and work exchange (as seen in [White1991]).

The deformation tensor is a second-order tensor and its matrix notation is

$$\boldsymbol{t} = \boldsymbol{nT} = \boldsymbol{n} \begin{pmatrix} \tau_{11} & \tau_{12} & \tau_{13} \\ \tau_{21} & \tau_{22} & \tau_{23} \\ \tau_{31} & \tau_{32} & \tau_{33} \end{pmatrix} . \tag{1.5.13}$$

The elements at the main diagonal are the normal stresses, the remaining elements are the shear stresses. If the fluid is at rest, the velocity is zero and the shear stresses have to vanish, solely the normal stresses remain. Thus, it is

$$\tau_{ij} = -p\delta_{ij}, \qquad \text{where} \qquad \delta_{ij} = \begin{cases} 1 & i = j, \\ 0 & i \neq j, \end{cases} \tag{1.5.14}$$

where the tensor δ_{ji} is the so-called *Kronecker-Delta*. This case equals the *hydrostatic pressure*

$$t_i = -pn_i, \tag{1.5.15}$$

where the pressure p which is independent of $\boldsymbol{n}$, is its absolute value. In general, the deformation tensor can be separated in

$$\tau_{ij} = -p\delta_{ij} + P_{ij}\,, \tag{1.5.16}$$

where P_{ij} determines the tensor of *frictional tension*. In all common fluids the applied shear is a function of the strain rate

$$\tau_{ij} = f(\epsilon_{ij}) \quad \text{with} \quad i, j = 1, 2, 3. \tag{1.5.17}$$

For the so-called *Newtonian fluids*, which are considered in this thesis, it is

$$\tau_{ij} = 2\mu\epsilon_{ij} = \mu\frac{du_j}{dx_i} \quad \text{with } i,j = 1,2,3 \tag{1.5.18}$$

and the dynamic viscosity μ [kg/ms]. The transport property of the dynamic viscosity μ yields a relation between momentum flux and velocity gradient. As a thermodynamic property it is dependent on temperature and pressure. Its properties are further discussed in section 1.9.

The easiest assumption for the variation of viscous stresses with strain rate is a linear law which was first stated by Sir George Gabriel Stokes in 1845 in form of three assumptions (see [Stokes1845] and [White1991], chapter 2, 2-4). Regarding the first assumption, the stress tensor τ_{ij} of a continuous fluid is a linear function of the strain rates ϵ_{ij}. Second, the fluid is isotropic, hence its properties are independent of direction. And third, if the strain rates are zero, the deformation law equals the hydrostatic pressure, which was already mentioned above. From these three assumptions, Stokes derived the following deformation law which is fulfilled for all gases and mostly fluids (see [White1991], chapter 2, 2-4)

$$\tau_{ij} = -p\delta_{ij} + \mu\left(\frac{\partial u_i}{\partial x_j} + \frac{\partial u_j}{\partial x_i}\right) + \lambda\left(\frac{\partial u_k}{\partial x_k}\right)\delta_{ij} = 0 \tag{1.5.19}$$

with the thermal conductivity λ. Stokes assumed, that the sum of the normal stresses $\tau_{xx}, \tau_{yy}, \tau_{zz}$ are also a tensor invariant, analogously to the invariants of the strain rate in equation (1.5.8). Then, the mechanical pressure p can be supposed to be

$$\bar{p} = -\frac{1}{3}(\tau_{xx}, \tau_{yy}, \tau_{zz})\,. \tag{1.5.20}$$

With the deformation law in (1.5.19), one obtains

$$\bar{p} = -\frac{1}{3}(\tau_{xx}, \tau_{yy}, \tau_{zz}) = p - \left(\lambda + \frac{2}{3}\mu\right)\left(\frac{\partial u_k}{\partial x_k}\right)\delta_{ij}\,. \tag{1.5.21}$$

From this expression follows, that the mean pressure in a deforming viscous fluid does not equal the thermodynamic pressure. Stokes solved this problem by assuming, that

$$\lambda + \frac{2}{3}\mu = 0\,. \tag{1.5.22}$$

Furthermore, the assumption of an incompressible fluid with

$$\left(\frac{\partial u_k}{\partial x_k}\right)\delta_{ij} = 0 \tag{1.5.23}$$

resolves the problem of inequality between both pressure terms. In compressible flows the problem is probably avoided, if the viscous normal stresses are negligible which is the case